J. Fluid Mech. (2013), *vol.* 717, *pp.* 281–292.
doi:10.1017/jfm.2012.572

Capillary breakup of a liquid torus

Hadi Mehrabian[1] **and James J. Feng**[1,2],†

[1]Department of Chemical and Biological Engineering, University of British Columbia, Vancouver, BC V6T 1Z3, Canada

[2]Department of Mathematics, University of British Columbia, Vancouver, BC V6T 1Z2, Canada

(Received 22 August 2012; revised 31 October 2012; accepted 17 November 2012; first published online 1 February 2013)

Capillary instability of a Newtonian liquid torus suspended in an immiscible Newtonian medium is computed using a Cahn–Hilliard diffuse-interface model. The main differences between the torus and a straight thread are the presence of an axial curvature and an external flow field caused by the retraction of the torus. We show that the capillary wave initially grows linearly as on a straight thread. The axial curvature decreases the growth rate of the capillary waves while the external flow enhances it. Breakup depends on the competition of two time scales: one for torus retraction and the other for neck pinch-off. The outcome is determined by the initial amplitude of the disturbance, the thickness of the torus relative to its circumference, and the torus-to-medium viscosity ratio. The linearly dominant mode may not persist till nonlinear growth and breakup. The numerical results are generally consistent with experimental observations.

Key words: breakup/coalescence, drops, low-Reynolds-number flows

1. Introduction

This study is motivated by the recent experiment of Pairam & Fernández-Nieves (2009) on the breakup of glycerol tori suspended in silicone oil. They observed that a torus can either shrink to a single droplet or break down into multiple droplets depending on the thickness of the torus relative to its circumference. There is a clear connection to the classical problem of Rayleigh–Tomotika instability of a straight, infinitely long filament. But here the dynamics involves two additional factors: the shrinkage of the torus driven by the curvature of the axis that runs along the centre of the curved filament, and the concomitant flow in the surrounding fluid.

Capillary breakup of liquid filaments is a classical problem in fluid mechanics (Sirignano & Mehring 2000; Eggers & Villermaux 2008). A long cylindrical liquid thread becomes linearly unstable to disturbances with a wavelength longer than the circumference of the thread $2\pi a$, a being the radius of the filament. The most unstable wavelength is $9.02a$ for an inviscid filament (Rayleigh 1878), and longer and dependent on the viscosity ratio for a viscous thread in a viscous surrounding fluid (Tomotika 1935). The capillary waves grow into the nonlinear regime and ultimately lead to breakup, and satellite drops may appear depending on the viscosity ratio (Tjahjadi, Stone & Ottino 1992). Thus, capillary breakup of long straight filaments is well understood.

† Email address for correspondence: jfeng@math.ubc.ca

In comparison, we have a rather limited knowledge of the stability of curved filaments. Experimentally, Pairam & Fernández-Nieves (2009) studied the retraction and breakup of Newtonian tori in a Newtonian surrounding liquid. McGraw *et al.* (2010) and Wu *et al.* (2010) further considered the breakup of nano-scale polymer and liquid metal rings on solid substrates. Several theoretical and numerical studies have appeared in the literature, and most of these have dealt with the more complicated situation of a liquid ring or torus in contact with a solid substrate. For instance, Wu (2003) computed the Rayleigh modes on a liquid ring spreading on a solid after impingement. Bostwick & Steen (2010) considered the static stability of the so-called torus lift, a liquid ring constrained by a solid ribbon in contact with part of the liquid surface. Nguyen *et al.* (2012) carried out molecular-dynamics and long-wave continuum simulations of the capillary breakup of a nano-scale liquid metal ring on a solid surface. Gomes (2002) computed the stability of a rotating toroidal gas bubble constrained between two concentric cylinders. The baseline situation, of a freely suspended torus in a quiescent medium, seems to have been studied only by Yao & Bowick (2011); they solved the Stokes flow during the contraction of the torus but did not investigate its capillary instability.

In this study we simulate the dynamics of a Newtonian torus suspended in a surrounding Newtonian liquid in three dimensions (3D). The numerical computations are based on a diffuse-interface formalism, with finite elements on an unstructured and adaptively generated grid. First we will study the linear growth of a sinusoidal disturbance on the torus and investigate the effect of the retraction and the axial curvature on the growth rate. Then we will examine the nonlinear instability and the final breakup into droplets. Finally the numerical results will be compared with the experiment.

2. Problem setup and methodology

Consider a Newtonian liquid torus of viscosity μ_t suspended in an immiscible Newtonian medium of viscosity μ_m. Initially the cross-section of the torus is a circle of radius a_0, and the axis through the centre of the cross-section is a circle of radius R_0. Hereafter, we refer to the curvatures due to R_0^{-1} and a_0^{-1} as the axial curvature and azimuthal curvature, respectively. Although non-varicose modes of instability are possible under external forcing, experiments have shown only varicose necking and breakup. Thus, we assume symmetry about the mid-plane of the torus, and only need to consider its top half. Furthermore, we can compute a half or a quarter of the top half for the growth of odd and even sinusoidal modes (figure 1). A sinusoidal perturbation of wavelength l_0 is imposed on the torus at the start:

$$(r - R_0)^2 + z^2 = a_0^2 \left[1 + \delta_0 \cos\left(\frac{2\pi R_0}{l_0}\theta\right)\right]^2, \tag{2.1}$$

where r, z, and θ show the surface of the torus in cylindrical coordinates, $k = 2\pi R_0/l_0$ is the number of waves along the circumference $2\pi R_0$, and δ_0 is the initial dimensionless amplitude. In presenting results, k will be called the *wavenumber*, though it differs from the usual sense of the word ($2\pi a_0/l_0$). We use the subscript 0 to indicate the initial condition. With contraction of the torus and growth of the disturbance, $a(t)$, $R(t)$, $l(t)$ and $\delta(t)$ all change in time.

The subsequent fluid flow is governed by the Stokes equation; inertia and buoyancy are negligible in the experiment and will be neglected in the computations. Since the interface will move, deform and eventually break up, the simulation requires

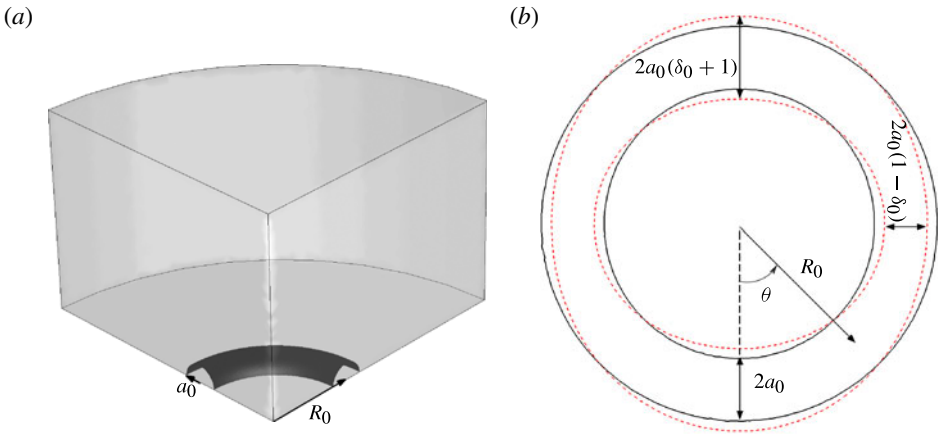

FIGURE 1. (Colour online) (*a*) A quarter of the top half of a liquid torus for simulating the capillary growth of an even mode, i.e. with an even number of wavelengths around the torus. For odd modes, a half of the top half must be used. (*b*) The interface on the symmetric mid-plane with and without a sinusoidal disturbance.

an interfacial capturing algorithm. We adopt a diffuse-interface Cahn–Hilliard model, in which the two fluid components are assumed to mix in a thin but continuous interfacial region of thickness ϵ. Thus the interfacial discontinuity is regularized, and the interfacial evolution, including breakup, can be simulated naturally. The coupled Stokes and Cahn–Hilliard equations are solved using a finite-element method on an adaptive unstructured grid. The theoretical model, numerical algorithm and detailed validations have been described by Zhou *et al.* (2010). The accuracy and efficiency of the method have been demonstrated by successful application to an array of interfacial flow problems (Yue *et al.* 2006*b*; Zhou, Yue & Feng 2007; Gao & Feng 2011*a*,*b*; Mehrabian & Feng 2011; Yue & Feng 2011*a*). Here we only note three salient points in the methodology (Zhou *et al.* 2010). First, the interfacial thickness ϵ has to be small enough so the numerical results no longer depend on it. This is known as the sharp interface limit. Second, the thin interface has to be adequately resolved by fine grids. This requirement is met in our method by local refinement and adaptive refining and coarsening upstream and downstream of the interface, respectively. Finally, the Cahn–Hilliard model introduces a diffusion length l_d. It is important to computing moving contact lines (Yue & Feng 2010, 2011*b*) and morphological changes such as coalescence and breakup (Yue, Zhou & Feng 2006*a*). The choice of its value is discussed below.

For boundary conditions, we assume symmetry on the bottom and planar sidewalls of the domain of figure 1(*a*). The top wall is $11a$ above the top of the torus, on which we impose zero stresses. The outer cylindrical wall is at least $10a$ from the torus, and is solid with vanishing velocity. The outer boundaries are sufficiently removed from the torus that they do not affect the retraction and capillary instability on it. Toward the end of the paper, when trying to match the experimental geometry of Pairam & Fernández-Nieves (2009), we will bring the sidewall closer to the torus.

Two dimensionless numbers quantify the physical problem: the torus-to-medium viscosity ratio $m = \mu_t/\mu_m$ and the initial aspect ratio of the torus $\beta = R_0/a_0$. The Cahn–Hilliard model introduces two more parameters: the Cahn number $Cn = \epsilon/a_0$ and a diffusion length scale $S = l_d/a_0$. We have used $S = 0.02$ and $Cn = 0.05$

throughout this paper; this ensures the attainment of the sharp interface limit during torus retraction. The final breakup involves length scales shrinking to zero, and the finite thickness of the interface and the diffusion within will eventually manifest themselves. With $Cn = 0.05$, numerical experiments show that the pinch-off time increases by less than 5 % when S decreases from 0.02 to 0.004. In presenting results, we use a_0 as the characteristic length and the capillary time $t_c = a_0\mu_t/\sigma$ as the characteristic time, σ being the interfacial tension. The wavelength l, however, will be scaled by the instantaneous circumference of the cross-section of the torus $2\pi a$ to facilitate comparison with the straight-filament results. Note that t_c characterizes the capillary waves on the torus. The retraction of the torus in the presence of a viscous external fluid is on the time scale $(R_0 - a_0)\mu_m/\sigma = t_c(\beta - 1)/m$.

3. Results: linear growth of capillary waves

Compared with the Rayleigh–Tomotika instability on a straight filament, several complications arise on the torus. First, due to the finite circumference of the torus, only a number of discrete wavelengths are possible for a given aspect ratio β. Second, the torus has an axial curvature (R^{-1}) which may affect the growth of the capillary wave. Finally, the contracting torus induces a flow in the surrounding fluid which may modify the capillary instability as well (Tomotika 1936; Mikami, Cox & Mason 1975). Under the constraint of quantized wavelengths, the last two effects will be explored separately.

3.1. *Quasi-static retraction: effect of axial curvature*

By choosing a large initial aspect ratio β and a small viscosity ratio m, we can separate the time scales for the growth of the capillary wave and the retraction of the torus. In physical terms, this corresponds to a thin torus retracting slowly in a highly viscous bath. The speed of retraction $\mathrm{d}R/\mathrm{d}t$ decreases in time. As an indication of its magnitude, $\mathrm{d}R/\mathrm{d}t = -0.0036$ at $R = 4$ for $m = 0.033$. For larger m, the retraction speed increases in proportion as expected. Such a quasi-static process is convenient in that we can probe the effect of the axial curvature on the linear instability of the torus while excluding the dynamic effect of the retraction-induced external flow. Furthermore, if we use a small enough initial perturbation and carry out the simulations on the time scale of torus retraction $t_c(\beta - 1)/m$, we can record the linear growth rate at different axial curvatures and wavelengths. Thus a dispersion relation can in principle be generated in one simulation.

For one such torus with initial aspect ratio $\beta = 5.3$ and viscosity ratio $m = 0.033$, we impose two wave forms on it ($k = 2$). Different initial amplitudes ($\delta_0 = 0.005$ and 0.01) are tested, and $\ln(\delta/\delta_0)$ initially grows linearly in time with a slope α that is independent of δ_0. This confirms that we are in the linear regime, with α being the growth rate. Over longer times (on the order of $t_c(\beta - 1)/m \sim 100t_c$), the growth rate remains independent of δ_0 but starts to change in time. This is an effect of the torus retraction even though the instability is still in the linear regime. Since the wavenumber $k = 2$ is fixed, the wavelength shrinks with the retraction, not only in dimensional terms, but also relative to the thickening filament radius a. Thus, recording the growth rate as a function of the changing wavelength produces the dispersion relation in figure 2(*a*). The growth rate on the torus is some 15 % below that on the straight filament, although the difference is expected to diminish for larger β. For $\beta \approx 10$, the difference narrows down to within 5 %. In the limit of $R_0 \gg a_0$, of course, one recovers the growth rate on a straight circular cylinder. Therefore,

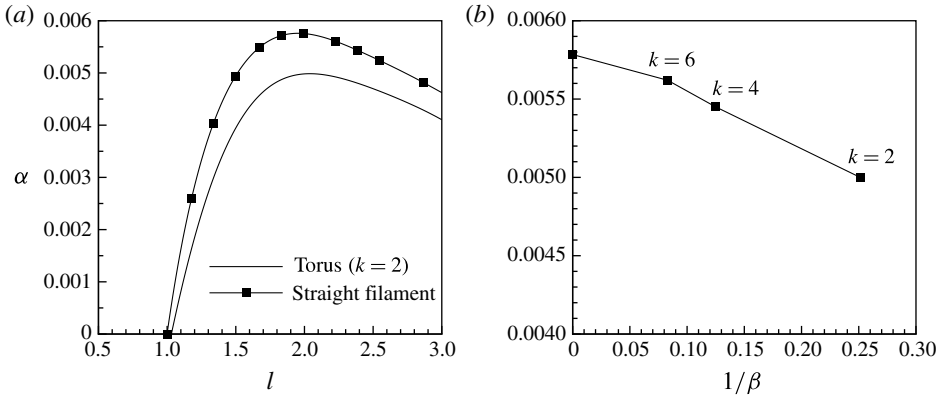

FIGURE 2. (*a*) Dispersion relation on a shrinking torus compared to that for a straight filament. The latter is computed by our diffuse-interface method and agrees with the Tomotika formula within 4 %. The wavelength l and the growth rate α are made dimensionless by the instantaneous $2\pi a$ and t_c, respectively. (*b*) The linear growth rate decreases with the axial curvature for a prescribed dimensionless wavelength $l_0 = 2$. The point at $1/\beta = 0$ corresponds to a straight filament.

the axial curvature on the torus tends to hinder the growth of the capillary waves. Note also that both the minimum wavelength for instability and the fastest growing wavelength have shifted slightly to longer waves from those for the straight filament.

The simulation above is not ideal in quantifying the effect of the axial curvature R^{-1} on the growth rate α since the former cannot be prescribed but continues to increase in time. For this purpose, we have conducted a series of simulations with tori of the same initial a_0, but different initial aspect ratio β in proportion to the wavenumber k. Thus, these capillary waves have the same initial wavelength (in dimensionless form $l_0 = (2\pi R_0/k)/(2\pi a_0) = \beta/k = 2$), and differ only in the axial curvature R_0^{-1}. Figure 2(*b*) plots the initial linear growth rate α as a function of $1/\beta = a_0 R_0^{-1}$, the non-dimensionalized axial curvature. It shows unequivocally that the instantaneous growth rate decreases with the axial curvature.

3.2. *Faster retraction: effect of external flow*

To examine the effect of the external flow field on capillary instability of the torus, we have gradually decreased the viscosity of the suspending fluid to produce faster retraction of the torus. Even on a straight filament, in the absence of the flow effect being examined, the ambient viscosity would have affected the growth rate. To remove this effect and isolate that of the retraction-induced external flow, we compute the ratio α_r between the growth rate on a retracting torus and that on a straight filament, the latter being calculated from the Tomotika formula using the same viscosities and the instantaneous filament diameter and wavelength of the torus. This ratio, as a function of m, demonstrates how the flow affects the growth of the instability. Note that the torus viscosity μ_t remains unchanged in this process; it gives a fixed time scale t_c against which the growth rate is measured. The faster retraction is then indicated by an increasing viscosity ratio m.

Figure 3(*a*) plots the ratio of growth rates α_r against the viscosity ratio m for a dimensionless wavelength $l = 2$. With increasing m and hence increasing retraction speed, the growth rate ratio increases. This implies that the external flow induced

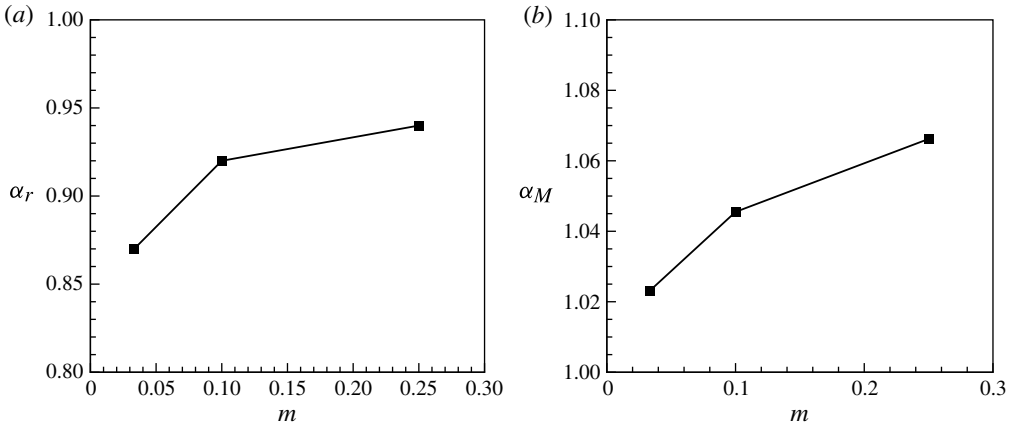

FIGURE 3. (*a*) Ratio between growth rate on a torus and that on a straight filament as a function of the viscosity ratio for a capillary wave of dimensionless wavelength $l = 2$. (*b*) Ratio of growth rates on a straight filament under uniform extensional flow, calculated from the theoretical result of Mikami *et al.* (1975).

by the torus retraction has the effect of enhancing the growth of instability. That α_r is below unity reflects the quasi-static effect of the axial curvature discussed in the preceding subsection.

It is interesting to compare this flow effect with that on a straight filament. Mikami *et al.* (1975) computed the effect of a uniform extensional flow on the capillary instability on a straight filament. The growth rate is written as the sum of two terms (see their equation (59)). The first, due to the thinning of the filament and advective lengthening of the wavelength, had previously been computed by Tomotika (1936). This effect is quasi-static in nature, and its counterpart on the torus has been included in the analysis of the last subsection. The second term, proportional to the strain rate G, explicitly accounts for the flow effect. From our torus retraction simulation, we extract a negative G from the rate of filament thickening, and then compute the two terms for the same wavelength $l = 2$. We take the ratio between the total growth rate and the first term, and plot it as a ratio of growth rates α_M in figure 3(*b*). This is not the same ratio as that in figure 3(*a*) since there is no axial curvature. Nevertheless, the qualitative trend is clear and confirms our observations on the retracting torus: the compression of a straight filament enhances the growth of capillary instability.

4. Results: nonlinear growth and breakup

The nonlinear instability and breakup of the torus must take place before the torus contracts onto itself. In this process, the quantized wavelength available and the initial amplitude of the perturbation are both important factors. Besides, the initial aspect ratio of the torus and the viscosity ratio are key parameters.

4.1. *Fastest mode*

On a retracting torus, with the wavelength and filament thickness changing continually, the initially dominant mode does not necessarily persist till breakup. In fact, the torus retraction should favour initially longer waves and this is illustrated in figure 4, with $\beta = 6.7$, $m = 0.033$ and $\delta_0 = 0.02$. Based on the dispersion relation for the torus, the linearly dominant wavelength is $l = 2.03$ and corresponds to a wavenumber $k = 3.3$.

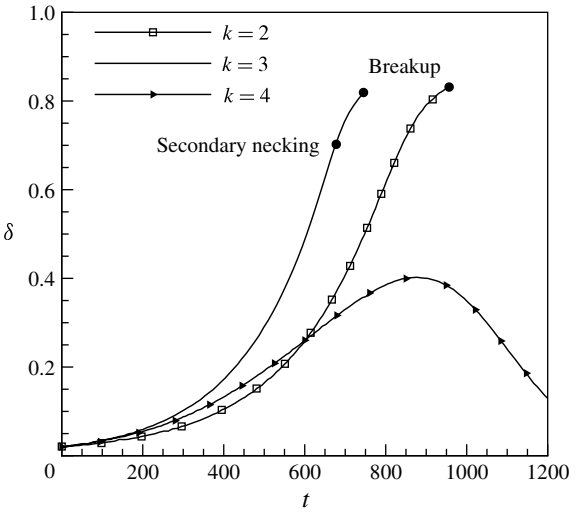

FIGURE 4. Nonlinear evolution of three modes of instability, with wavenumber $k = 2$, 3 and 4, for $\beta = 6.7$, $m = 0.033$ and initial amplitude $\delta_0 = 0.02$; δ is the instantaneous amplitude of the capillary waves. The curves for $k = 2$ and $k = 3$ end in breakup, with the onset of secondary necking also marked on the latter. The $k = 4$ mode ends in complete retraction.

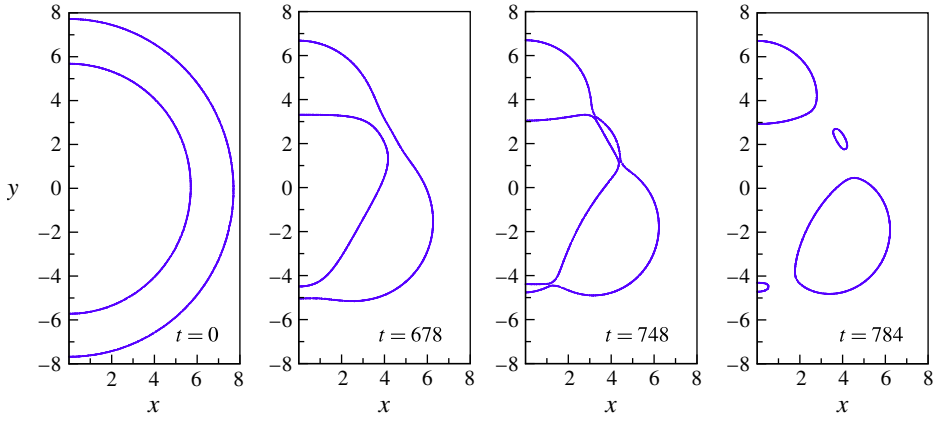

FIGURE 5. (Colour online) Snapshots of the evolving interface on the mid-plane of the torus for $\beta = 6.7$, $m = 0.033$ and $\delta_0 = 0.02$. The interface is given by the level set of $\phi = 0$.

Thus, $k = 3$ or $k = 4$ should initially produce the fastest growth. Indeed, the two modes grow at comparable rates at the beginning. But as the torus shrinks, the $k = 3$ mode maintains a high growth rate while the growth rate for $k = 4$ declines, leading eventually to retraction, not breakup. This can be rationalized by noting that for a retracting torus with a fixed wavenumber k, the wavelength gets shorter in time, in dimensional terms and especially relative to the growing thickness a. Thus the initially longer wave ($k = 3$) is favoured over the shorter one ($k = 4$). The $k = 2$ mode grows more slowly but does lead to breakup.

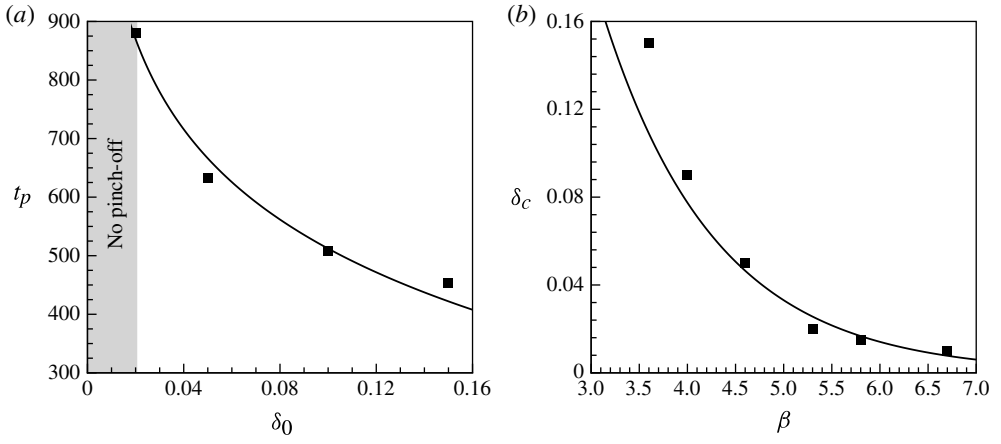

FIGURE 6. (*a*) The pinch-off time decreases with increasing initial amplitude of disturbance. $\beta = 5.3$, $m = 0.033$, $k = 2$. The solid curve is the best fitting by (4.1). (*b*) The critical initial amplitude δ_c decreases with the initial aspect ratio β. The solid curve is the best fitting by (4.2).

The breakup of the torus into droplets is depicted by snapshots in figure 5 for $k = 3$, starting from an initial perturbation of amplitude $\delta_0 = 0.02$. Primary necking proceeds at three points around the circumference of the torus until $t = 678$, when two secondary necks emerge around each primary neck. At $t = 748$ the torus breaks down into three primary drops and three satellite droplets. In time these all relax toward a spherical shape.

4.2. *Pinch-off time versus retraction time*

From the preceding discussion, it is clear that the breakup of the torus depends on the competition of two time scales: t_p needed for the neck to pinch off, and t_s needed for the torus to shrink onto itself. This competition can be affected by multiple factors. For example, the $k = 4$ mode of figure 4 can survive till breakup if the initial perturbation has a sufficiently large amplitude; δ_0 defines t_p. Besides, the breakup depends on the initial aspect ratio β and the viscosity ratio m, each having a role in t_s. These three factors will be examined in turn.

Figure 6(*a*) demonstrates the dependence of the pinch-off time t_p on the initial amplitude δ_0 for $\beta = 5.3$, $m = 0.033$ and $k = 2$, which is the initially dominant mode. If δ_0 is below a critical value $\delta_c \approx 0.02$, no breakup occurs. For $\delta_0 > \delta_c$, the torus breaks up into two principal drops and two satellite droplets, and t_p decreases with increasing δ_0 as expected. Besides, the faster the breakup, the larger the satellite droplets. The critical amplitude δ_c decreases with increasing initial aspect ratio β, as shown in figure 6(*b*). The thinner, longer torus offers a longer t_s within which breakup can take place. In the β range shown, $k = 2$ persists till breakup for all $\delta_0 > \delta_c$; no other modes emerge from noise to overtake the imposed $k = 2$ mode.

The viscosity ratio $m = \mu_t/\mu_m$ is another parameter that modulates the competition between pinch-off and retraction. Our results show that the torus retraction is more influenced by the matrix viscosity μ_m while the necking and pinch-off more by the torus viscosity μ_t. As m increases from 0.033 to 0.05 and 0.1, the critical amplitude δ_c increases from 0.02 to 0.03 and 0.07. For $m = 0.5$ even $\delta_0 = 0.18$ is unable to

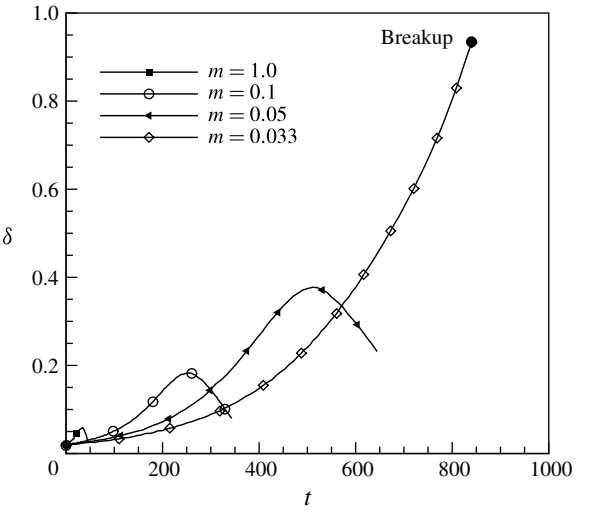

FIGURE 7. Effect of the viscosity ratio on the growth of disturbance. $\beta = 5.3$, $\delta_0 = 0.02$ and $k = 2$.

break down the relatively viscous torus before it contracts into a single drop, often entrapping a droplet of the ambient fluid in the centre (Yue *et al.* 2006*b*).

Figure 7 illustrates the effect of m on the growth of an initial disturbance with $k = 2$, which is the initially dominant mode for all the m values considered here. Since time is scaled by $t_c = a_0\mu_t/\sigma$, using the torus viscosity, increasing m can be conveniently thought of as due to a decreasing μ_m. As μ_m decreases, the initial growth rate of the capillary wave increases. However, the retraction of the torus becomes faster as well. Numerical experiments show that the latter has the upper hand. Thus, for lower μ_m, δ reaches a maximum quickly and then declines, due to the thickening of the torus and the effective shortening of the wavelength. It is for the largest matrix viscosity, at $m = 0.033$, that the slow retraction offers the capillary disturbance sufficient time to grow till breakup, despite the slower linear growth rate.

The competition between time scales can be represented by scaling arguments. As noted earlier, the shrinkage time $t_s \sim t_c(\beta - 1)/m$. The pinch-off time can be taken as that required for the disturbance to grow from the non-dimensionalized initial amplitude δ_0 to 1: $t_p = -\ln\delta_0/\alpha_m$, where the fastest growth rate α_m can be estimated from the Tomotika solution: $\alpha_m \sim \sqrt{m}/t_c$ (Cohen *et al.* 1999). Therefore, we can write

$$t_p = t_c \frac{c_1}{\sqrt{m}} \ln\left(\frac{1}{\delta_0}\right), \tag{4.1}$$

and $c_1 = 40.6$ gives a reasonably good fitting to the numerical data in figure 6(*a*). Furthermore, equating this t_p with the shrinkage time t_s gives us the critical initial amplitude for breakup:

$$\delta_c = \exp\left(-c_2 \frac{\beta - 1}{\sqrt{m}}\right), \tag{4.2}$$

which fits the data in figure 6(*b*) well with $c_2 = 0.16$. Given that much of the necking and pinch-off is nonlinear, these linearly based scaling relationships work remarkably well.

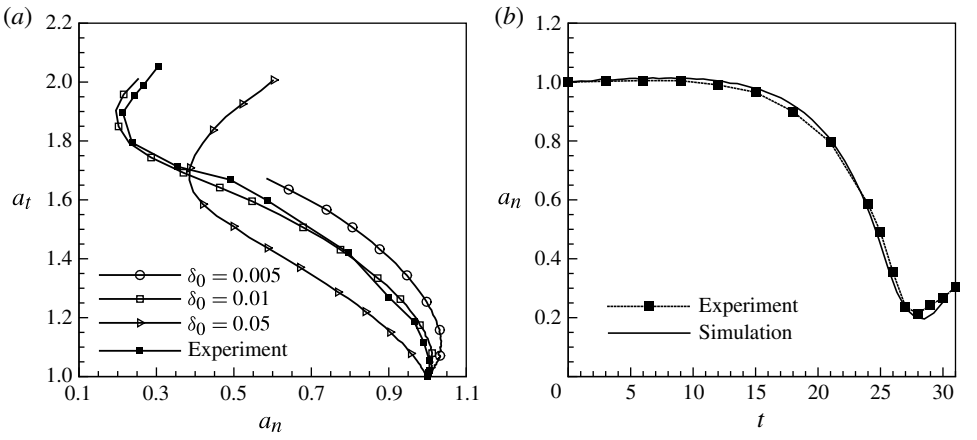

FIGURE 8. (*a*) Determining the initial amplitude of perturbation δ_0 from the variation of the thickest radius a_t versus the thinnest radius a_n on the torus. Both radii are normalized by the initial value a_0. (*b*) Determining the interfacial tension σ from the temporal variation of a_n. $\beta = 5.3$, $k = 2$ and $m = 0.033$.

5. Comparison with experiment

As far as we know, the only prior experiment on the breakup of a freely suspended torus is that of Pairam & Fernández-Nieves (2009). With Newtonian glycerol tori in a Newtonian oil bath, these authors reported that thick tori shrink to one droplet while thin ones break down into a number of droplets through Rayleigh–Tomotika instability. We match the liquid viscosities and flow geometry in the experiment, where the torus is confined in a cylindrical drum, with the top and sidewalls being some $6a$ away from the outer edge of the torus. Our numerical experimentation shows that this confinement is essential for slowing down the torus retraction and allowing breakup. Still two uncertainties complicate a direct comparison. The first is the initial amplitude of perturbation δ_0. In the experiment, the torus is generated by releasing a glycerine jet into silicone oil while the drum rotates. There is a complex flow history, and it is not obvious how to gauge the magnitude of the initial perturbation. The second is the interfacial tension σ in the experiment. It was not reported and cannot be made available to us. We determine δ_0 and σ first by fitting the experimental data.

First note that the capillary time t_c is the only time scale of the problem, and the only role of σ is to lengthen or compress t_c. Thus, in figure 8(*a*) we plot the radius a_t of the thickest part of the torus against the thinnest radius a_n at the neck. Such a curve should be independent of t_c. Among numerical results starting from different δ_0 values, $\delta_0 = 0.01$ agrees very closely with the experiment. So we take $\delta_0 = 0.01$ to be the initial amplitude for this case. Now plotting the temporal variation of the neck radius in figure 8(*b*) gives us a fitting of $\sigma = 31.8$ mN m^{-1}, close to handbook values (Pizzi & Mittal 2003).

With the δ_0 and σ values determined, we compare the number of primary drops N between the simulation and the experiment for a range of torus aspect ratio β (figure 9). All the simulations have started with the fastest linear mode for the β value. The results agree with the experiment except for $\beta = 4$, where the simulation predicts complete retraction, while the experiment reported $N = 1$, breakup at a single primary neck for the $k = 1$ mode. We cannot explain this at present; possibly this

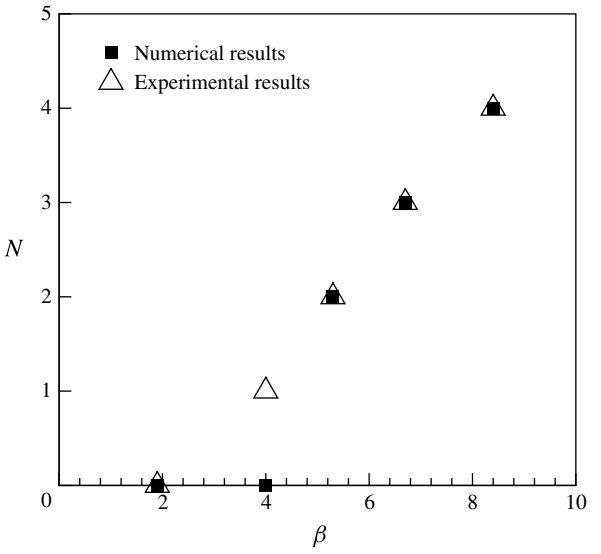

FIGURE 9. Comparison between the predicted and observed number of primary drops after breakup, for tori with five initial aspect ratios β; $m = 0.033$ and $\delta_0 = 0.01$. $N = 0$ and 1 refer to, respectively, complete retraction with no breakup and breakup at a single primary neck.

experiment had a different δ_0 from that fitted in figure 8(*a*) for $\beta = 5.3$. Numerical experimentation indicates that $\delta_0 = 0.02$ would lead to breakup at a single neck. In all the cases leading to breakup, N corresponds to the fastest linear mode. Even though the wavelength and filament thickness both change during the retraction, we have never seen the linearly dominant mode yielding to a nascent mode in the nonlinear stage. This reflects the fact that there is a limited time window for growth and it is too short for another mode to emerge spontaneously from random noise.

Acknowledgements

This research was partially supported by the NSERC, the Canada Research Chair program and the Canada Foundation for Innovation. We acknowledge discussions with G. Ghigliotti, E. Pairam and Q. Wang.

REFERENCES

BOSTWICK, J. B. & STEEN, P. H. 2010 Stability of constrained cylindrical interfaces and the torus lift of Plateau–Rayleigh. *J. Fluid Mech.* **647**, 201–219.

COHEN, I., BRENNER, M. P., EGGERS, J. & NAGEL, S. R. 1999 Two fluid drop snap-off problem: experiments and theory. *Phys. Rev. Lett.* **83**, 1147–1150.

EGGERS, J. & VILLERMAUX, E. 2008 Physics of liquid jets. *Rep. Prog. Phys.* **71**, 036601.

GAO, P. & FENG, J. J. 2011*a* A numerical investigation of the propulsion of water walkers. *J. Fluid Mech.* **668**, 363–383.

GAO, P. & FENG, J. J. 2011*b* Spreading and breakup of a compound drop on a partially wetting substrate. *J. Fluid Mech.* **682**, 415–433.

GOMES, D. A. 2002 Stability of rotating liquid films. *Q. J. Mech. Appl. Maths* **55**, 327–343.

MCGRAW, J. D., LI, J., TRAN, D. L., SHI, A.-C. & DALNOKI-VERESS, K. 2010 Plateau–Rayleigh instability in a torus: formation and breakup of a polymer ring. *Soft Matt.* **6**, 1258–1262.

MEHRABIAN, H. & FENG, J. J. 2011 Wicking flow through microchannels. *Phys. Fluids* **23**, 122108.

MIKAMI, T., COX, R. G. & MASON, S. G. 1975 Breakup of extending liquid threads. *Intl J. Multiphase Flow* **2**, 113–138.

NGUYEN, T. D., FUENTES-CABRERA, M., FOWLKES, J. D., DIEZ, J. A., GONZÁLEZ, A. G., KONDIC, L. & RACK, P. D. 2012 Competition between collapse and breakup in nanometre-sized thin rings using molecular dynamics and continuum modelling. *Langmuir* **28**, 13960–13967.

PAIRAM, E. & FERNÁNDEZ-NIEVES, A. 2009 Generation and stability of toroidal droplets in a viscous liquid. *Phys. Rev. Lett.* **102**, 234501.

PIZZI, A. & MITTAL, K. L. 2003 *Handbook of Adhesive Technology*. Marcel Dekker.

RAYLEIGH, LORD 1878 On the instability of jets. *Proc. Lond. Math. Soc.* **10**, 4–13.

SIRIGNANO, W. A. & MEHRING, C. 2000 Review of theory of distortion and disintegration of liquid streams. *Prog. Energy Combust. Sci.* **26**, 609–655.

TJAHJADI, M., STONE, H. A. & OTTINO, J. M. 1992 Satellite and subsatellite formation in capillary breakup. *J. Fluid Mech.* **243**, 297–317.

TOMOTIKA, S. 1935 On the instability of a cylindrical thread of a viscous liquid surrounded by another viscous fluid. *Proc. R. Soc. Lond.* A **150**, 322–337.

TOMOTIKA, S. 1936 Breaking up of a drop of viscous liquid immersed in another viscous fluid which is extending at a uniform rate. *Proc. R. Soc. Lond.* A **153**, 302–318.

WU, Y., FOWLKES, J. D., RACK, P. D., DIEZ, J. A. & KONDIC, L. 2010 On the breakup of patterned nanoscale copper rings into droplets via pulsed-laser-induced dewetting: competing liquid-phase instability and transport mechanisms. *Langmuir* **26**, 11972–11979.

WU, Z.-N. 2003 Approximate critical Weber number for the breakup of an expanding torus. *Acta Mech.* **166**, 231–239.

YAO, Z. & BOWICK, M. 2011 The shrinking instability of toroidal liquid droplets in the Stokes flow regime. *Eur. Phys. J. E* **34**, 1–6.

YUE, P. & FENG, J. J. 2010 Sharp interface limit of the Cahn–Hilliard model for moving contact lines. *J. Fluid Mech.* **645**, 279–294.

YUE, P. & FENG, J. J. 2011*a* Can diffuse-interface models quantitatively describe moving contact lines? *Eur. Phys. J. – Spec. Top.* **197**, 37–46.

YUE, P. & FENG, J. J. 2011*b* Wall energy relaxation in the Cahn–Hilliard model for moving contact lines. *Phys. Fluids* **23**, 012106.

YUE, P., ZHOU, C. & FENG, J. J. 2006*a* A computational study of the coalescence between a drop and an interface in Newtonian and viscoelastic fluids. *Phys. Fluids* **18**, 102102.

YUE, P., ZHOU, C., FENG, J. J., OLLIVIER-GOOCH, C. F. & HU, H. H. 2006*b* Phase-field simulations of interfacial dynamics in viscoelastic fluids using finite elements with adaptive meshing. *J. Comput. Phys.* **219**, 47–67.

ZHOU, C., YUE, P. & FENG, J. J. 2007 The rise of Newtonian drops in a nematic liquid crystal. *J. Fluid Mech.* **593**, 385–404.

ZHOU, C., YUE, P., FENG, J. J., OLLIVIER-GOOCH, C. F. & HU, H. H. 2010 3D phase-field simulations of interfacial dynamics in Newtonian and viscoelastic fluids. *J. Comput. Phys.* **229**, 498–511.